A&A 380, 665–672 (2001)
DOI: 10.1051/0004-6361:20011498

Astronomy & Astrophysics

A search for massive dense cores with ^{13}CO $J = 1$–0 line*

Y. Wu, J. Wu, and J. Wang

Astronomy Department, CAS-PKU Joint Beijing Astrophysics Center, Peking University, Beijing 100871, PR China

Received 31 January 2001 / Accepted 15 October 2001

Abstract. This paper reports ^{13}CO $J = 1$–0 line observations toward 107 IRAS or H_2O maser sources with the 13.7 m telescope of the Purple Mountain Observatory (PMO). Parameters of emission components are obtained and the profile characteristics are identified. For all the components, kinematic distances are derived. The bolometric luminosities of the corresponding IRAS sources are calculated for 95 sources, all of which are larger than 10^3 $L_{\odot}$. We also mapped eight sources. Results show that there are cores in the clouds. The sizes of the cores are about 1∼3 pc, much greater and more extensive than those of cores in dark clouds. The hydrogen densities are $\sim 10^2$–10^3 cm^{-3}. Systematic velocity shifts were found in 3 sources. Every mapped core contains one or more IRAS source. Each core has one and only one IRAS source that satisfies the criteria of ultra compact HII (UC HII) regions. For the cores, 2MASS data are available; dozens of 2MASS sources with different color indices and brightness are found within the core.

Key words. star: formation – ISM: clouds – ISM: kinematics and dynamics

1. Introduction

The studies of high-mass star formation greatly lag behind those of low-mass stars. Unlike low-mass cloud cores, massive star formation regions are usually located far away. They tend to produce stars in clusters, and evolve quickly. All these add complexity to the environment of high-mass cores, which inevitably attribute to the difficulty of exploring the dynamics and evolutionary states of massive star formation regions. Up to now, some typical formation indicators, such as outflows and collapse, are still poorly reported in high-mass cases. According to available statistics, the distribution of the known outflows with the bolometric luminosity of the driving YSOs (Wu et al. 1996) shows that there is a peak at 1∼10 $L_{\odot}$. More than ten protostellar collapse sources were found in low-mass cores while only 1–2 cases have been reported in high-mass star formation regions (Zhou 1999; Zhang et al. 1998). Since the early 1990s, efforts have been made in surveys of massive cores and outflows (Lada 1992; Churchwell 1993; Tatematsu et al. 1993; Li et al. 1997; Bronfman et al. 1996; Shephtrd & Churchwell 1996). By 1996, 250 massive YSOs had been catalogued (Chan 1996), yet it is still too few compared to the thousands of low mass sources, and many more samples are needed.

To search for relatively isolated high mass star formation regions and study the activities of YSOs, we chose strong or red IRAS sources (with $f > 100$ Jy at 100 μm or $\mathrm{Log}(F_{25}/F_{12}) > 0.57$, $\mathrm{Log}(F_{60}/F_{12}) > 1.30$, Wood & Churchweel 1989) or water masers as guides to carry out a survey with the ^{13}CO $J = 1$–0 line. In this paper we report the observation results, including the survey of 107 sources and maps of 8 sources. Among our samples there are 16 sources in the list of Chan (1996), but there are no reports of ^{13}CO measurement on these sources.

2. Observations

The ^{13}CO $J = 1$–0 (110.20135GHz) survey was made with the 13.7 m telescope at the Qinghai station of PMO in December of 1998. The beam size at this wavelength was 55″. The pointing and tracking accuracy were better than 10″. Jupiter and Mars were used as pointing checking sources.

An SIS receiver was employed. The system noise temperature including the atmosphere temperature at the zenith is 250 K (SSB). The backend is an AOS with 168.6 MHz total bandwidth and 1024 channels. The spectral resolution is 250 KHz (0.68 km s^{-1} at 110 GHz). The atmosphere temperature was used as the calibrator of antenna temperature T_{A}^{*}, which was corrected for the atmosphere absorption, antenna cover loss, radiation loss and

Send offprint requests to: Y. Wu,
e-mail: ywu@vega.bac.pku.edu.cn

* Table 1 is only available in electronic form at the CDS via anonymous ftp to cdsarc.u-strsbg.fr (130.79.128.5) or via
http://cdsweb.u-strasbg.fr/cgi-bin/qcat?J/A+A/380/665

rearward scattering and spillover. The radiation temperature $T_{\rm R} = T_{\rm A}^*/\eta_{\rm c}\eta_{\rm fss}$ (Kutner & Ulich 1981). Here $\eta_{\rm c}$ is the coupling efficiency of the antenna to the source, for our sources $\eta_{\rm c} = 1$; $\eta_{\rm fss}$ is the forward spillover and scattering efficiency, in this wavelength band $\eta_{\rm fss} = 61\%$. The system noise level is 0.1 K at the 0.68 km s^{-1} resolution with an efficient integration time of 2 min.

The position switch mode was adopted for all the spectral measurements. The integrating time is 4∼8 min per position. The offset position was usually a point about one degree away from the reference position of the source (Table 1). If it did not succeed at one point, another point was tested in another direction. Normally a clear ^{13}CO offset position was found in two or three trials.

For the maps the absolute position switch mode was used. The map was 5×5 with a step of 55″. Then if the line was still strong on the border of the map, mapping was extended until the line intensity reached less than or nearly half of the maximum value.

3. Survey results and discussion

The ^{13}CO $J = 1$–0 emission was detected in all the observed sources. The lines were fitted with a Gaussian function. Observed parameters including antenna temperature $T_{\rm A}{}^*$, $V_{\rm LSR}$ and line width $\Delta V_{\rm FWHM}$ of each component were obtained. The line profiles of nearly half of the sources are asymmetric. They have a visible departure from a Gaussian shape. Such a shape found in an optical thin line like ^{13}CO line is important, since it is a clue for supersonic bulk motion, especially outflows, in molecular clouds (Lada 1985). A statistic based in Table 1 of Myers et al. (1983) and the Catalogue of outflows (Wu et al. 1996) shows that about 40% of the non-Gaussian sources of Myers et al. (1983) were identified as outflows or outflow candidates. So we distinguish between different non-Gaussian profiles with the following characters, as shown in Fig. 1:

a: blue wing; b: red wing; c: wings or pedestal; d: flat top; e: emission peak skewed to low velocity; f: emission peak skewed to high velocity; g: double peak; h: two components.

Table 1 presents the observational results. Columns 2–5 give the equatorial coordinates and the Galactic coordinates, respectively. The line parameters $T_{\rm A}^*$, $V_{\rm LSR}$ and $\Delta V_{\rm FWHM}$ are shown in Cols. 6–8. Column 9 presents the characteristics of the profile. Columns 10–11 list the distance from the galactic center (R) and the kinematic distance (D) which were derived with the observed velocities according to Wouterloot & Brand (1989). For sources inside the solar circle, if two distances are generated by the calculation we took the closer one to estimate the luminosity of the source. For 12 sources, their locations are in the center or anti-center direction, their distances were very uncertain and are not presented. We also give the IRAS parameter of the sources. For water masers, the associated IRAS source was searched for within a $5' \times 5'$ region and the nearest one was chosen. The color indices $\mathrm{Log}(F_{25}/F_{12})$ and $\mathrm{Log}(F_{60}/F_{12})$ are listed in Cols. 12–13. Column 14 presents the bolometric luminosity which was calculated with the formulation in Casoli et al. (1986):
$L_{5-1000\mu{\rm m}} = 4\pi D^2 \times 1.75(F_{12}/0.79 + F_{25}/2 + F_{60}/3.9 + F_{100}/9.9)$,
where D is the distance listed in Col. 11. Henning et al. (1990) had demonstrated that such calculated luminosity $L_{\rm bol}$ is a good approximation to the bolometric luminosity. The $L_{\rm bol}$ is available for 95 sources. All of them have $L_{\rm bol} > 10^3\ L_\odot$ and can be generally classified as high mass sources (Wynn-Williams 1982).

Sources in this survey have larger line widths of 3.50 km s^{-1} on average, while the average line width of the dense cores are 1.3 km s^{-1} in Myers et al. (1983). For the samples of dense cores in Myers et al. (1983), some are associated with no sources and some are associated with much weaker sources ($L_{\rm IRAS} < 100\ L_\odot$, Beichman et al. 1986) than the sources in this paper.

4. Mapping results and discussion

Eight sources were mapped. The results show that all of them have cores. The emission intensity was integrated and the contour maps were presented in Figs. 2–9. The major and minor sizes a and b were taken from the contour with about two third of the maximum. The linear size s is $\frac{\sqrt{ab}}{2}$.

To obtain the ^{13}CO column density we use the CO data in Wouterloot & Brand (1989) and the observational data we obtained in Sep. 1997 and Dec. 1999 using the same equipment. For sources for which CO data are not available, we observed C^{18}O $J = 1$–0 at the reference position (see Table 1) with the same equipment. The column density of ^{13}CO is calculated under a local thermal equilibrium assumption according to Lada (1985). The column density of C^{18}O is obtained by the formula in Myers et al. (1983).

The parameters of the cores are listed in Table 2. Columns 2–3 list the major and minor angular sizes, respectively. Column 4 lists the linear size. The optical depth, excitation temperature and column density of ^{13}CO are presented in Cols. 5–7, and the corresponding parameters of C^{18}O are in Cols. 8–10. The density of hydrogen molecules is listed in Col. 11 and core mass in Col. 12.

In IRAS 06291–0421, G35.2–0.74S, and K47 we found a systematic shift of the line center velocity. For these sources we present a velocity-position diagram and velocity contours and calculate their gradients. All the mapped sources are noted individually as the following.

IRAS 06291+0421: the systematic velocity shift of ^{13}CO $J = 1$–0 is from NE to SW (Figs. 2a and 2d). The velocity gradient is 0.5 km s^{-1}/pc. If it is caused by a rotation, the spin angular velocity will be 1.6×10^{-14} s^{-1}.

IRAS 07207–1435: the peak of the core is near IRAS 07207–1435. Thirty-eight 2MASS sources are found within 1′ of this IRAS source. These 2MASS sources are

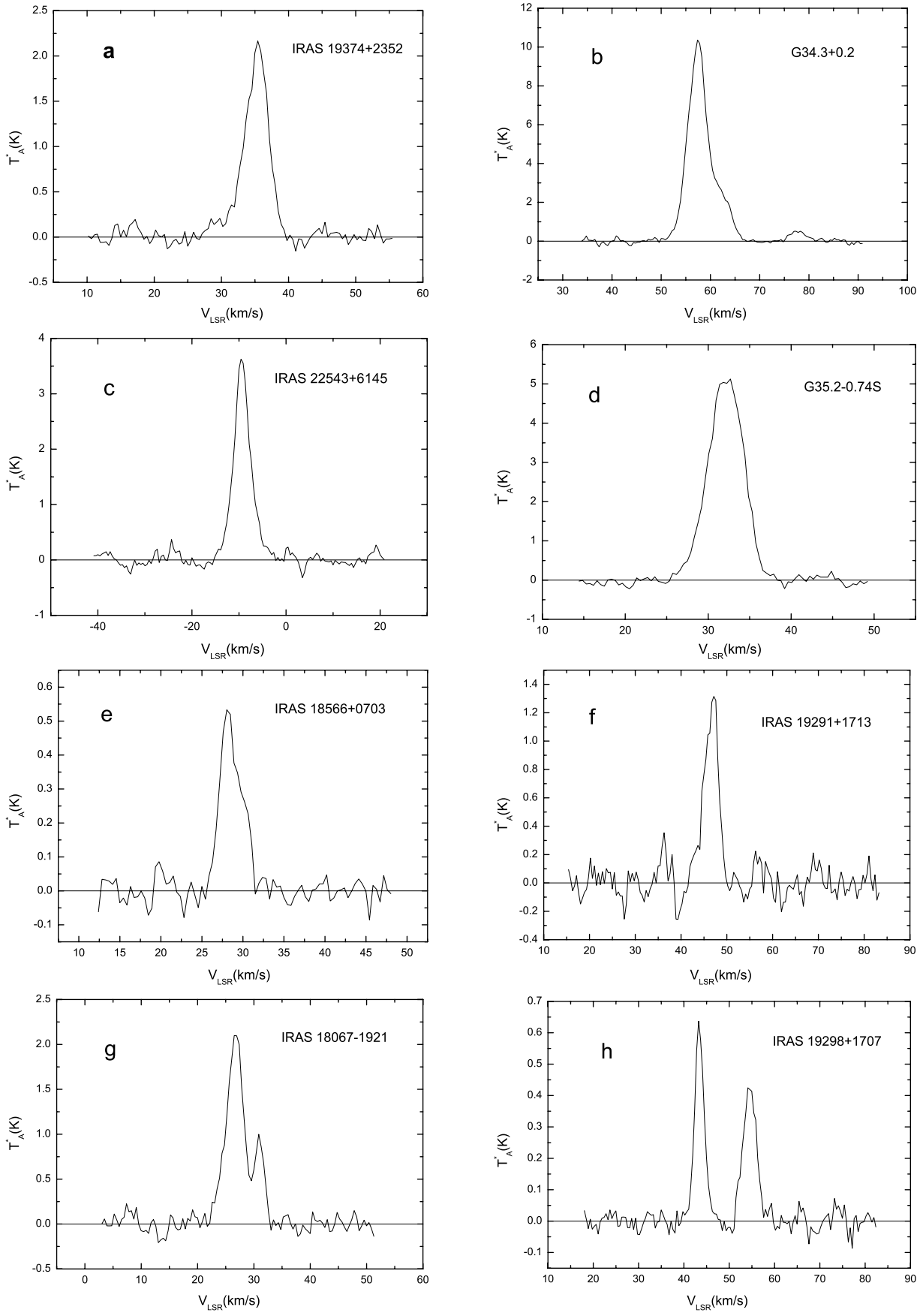

Fig. 1. Examples of ^{13}CO $J = 1$–0 spectra with non-Gaussian profiles. The classes labelled with **a)**–**h)** are described in Sect. 3.

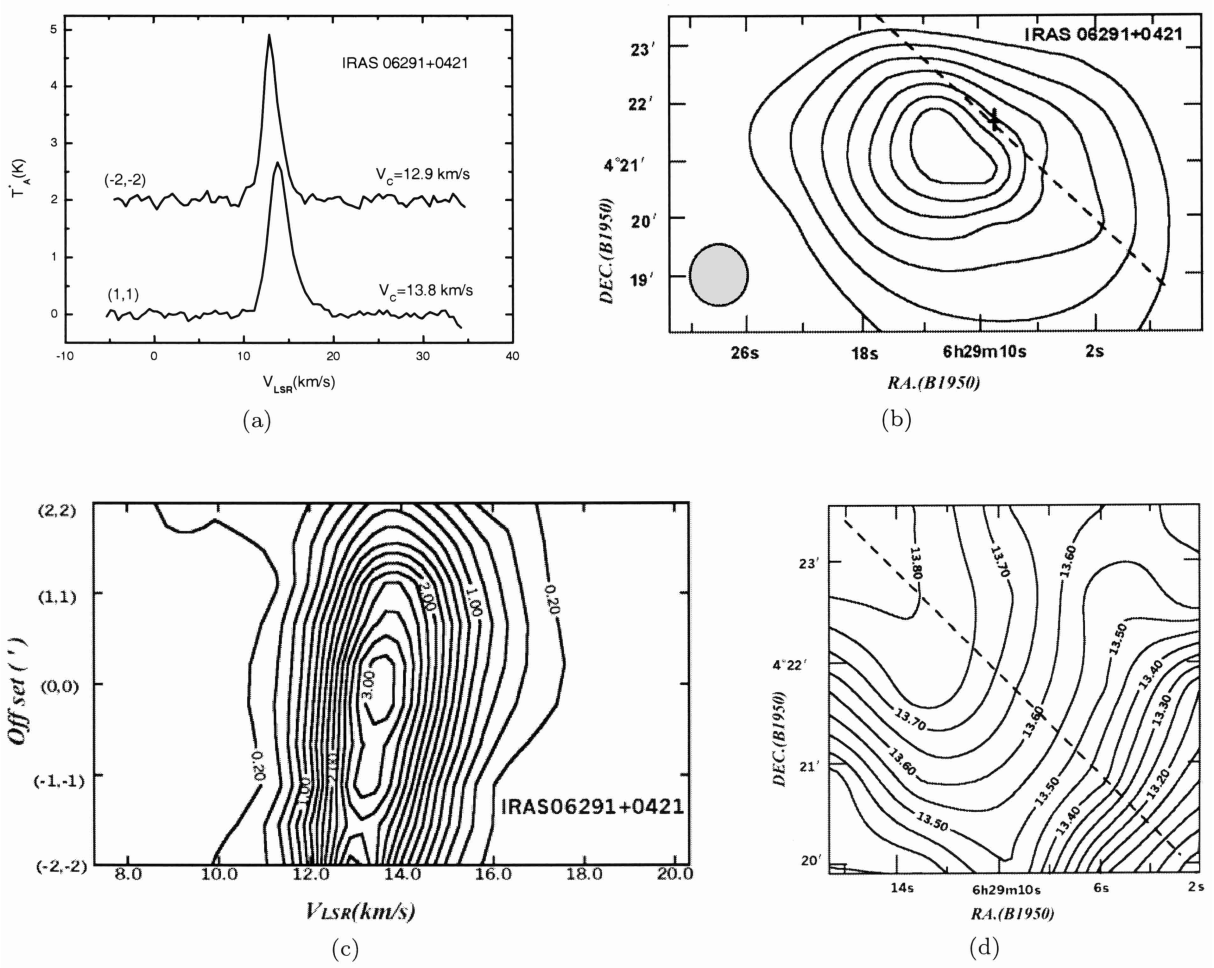

Fig. 2. IRAS 06291+0421: panel **a)**: ^{13}CO $J = 1$–0 spectra; panel **b)**: contours of total ^{13}CO $J = 1$–0 emission intensity. Contour lines begin from 15 K km s^{-1} with increasing step of 5 K km s^{-1}. The cross denotes the IRAS position with its scale reflecting the uncertainty ellipse; panel **c)**: position versus velocity plot; panel **d)**: line center velocity contours.

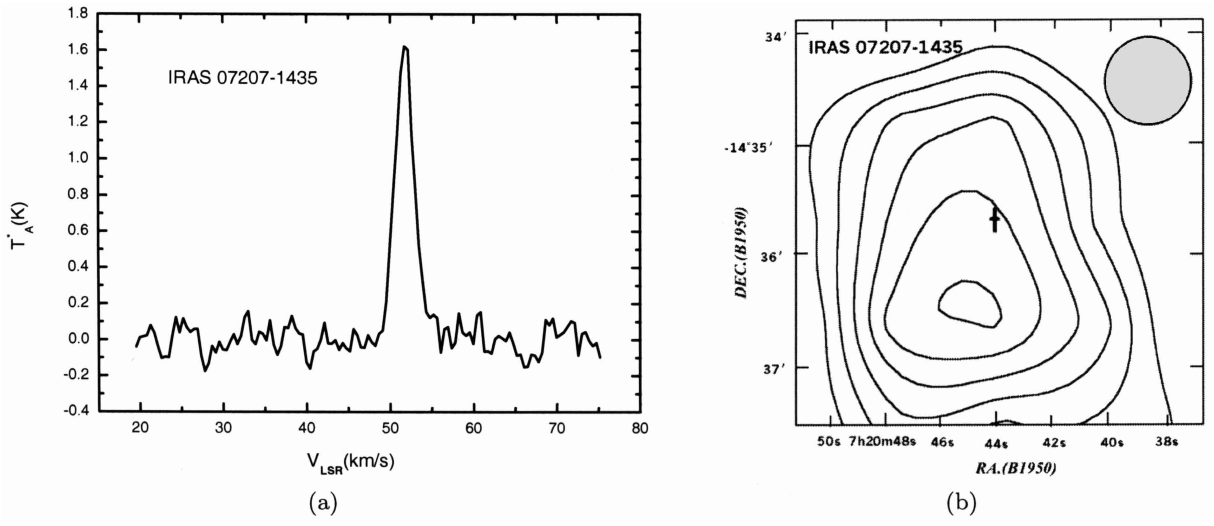

Fig. 3. IRAS 07207–1435: panel **a)**: ^{13}CO $J = 1$–0 spectra; panel **b)**: contours of total ^{13}CO $J = 1$–0 emission. Contour lines begin from 12 K km s^{-1} with increasing step of 2 K km s^{-1}. The cross symbol denotes the IRAS source with its scale reflecting the uncertainty ellipse.

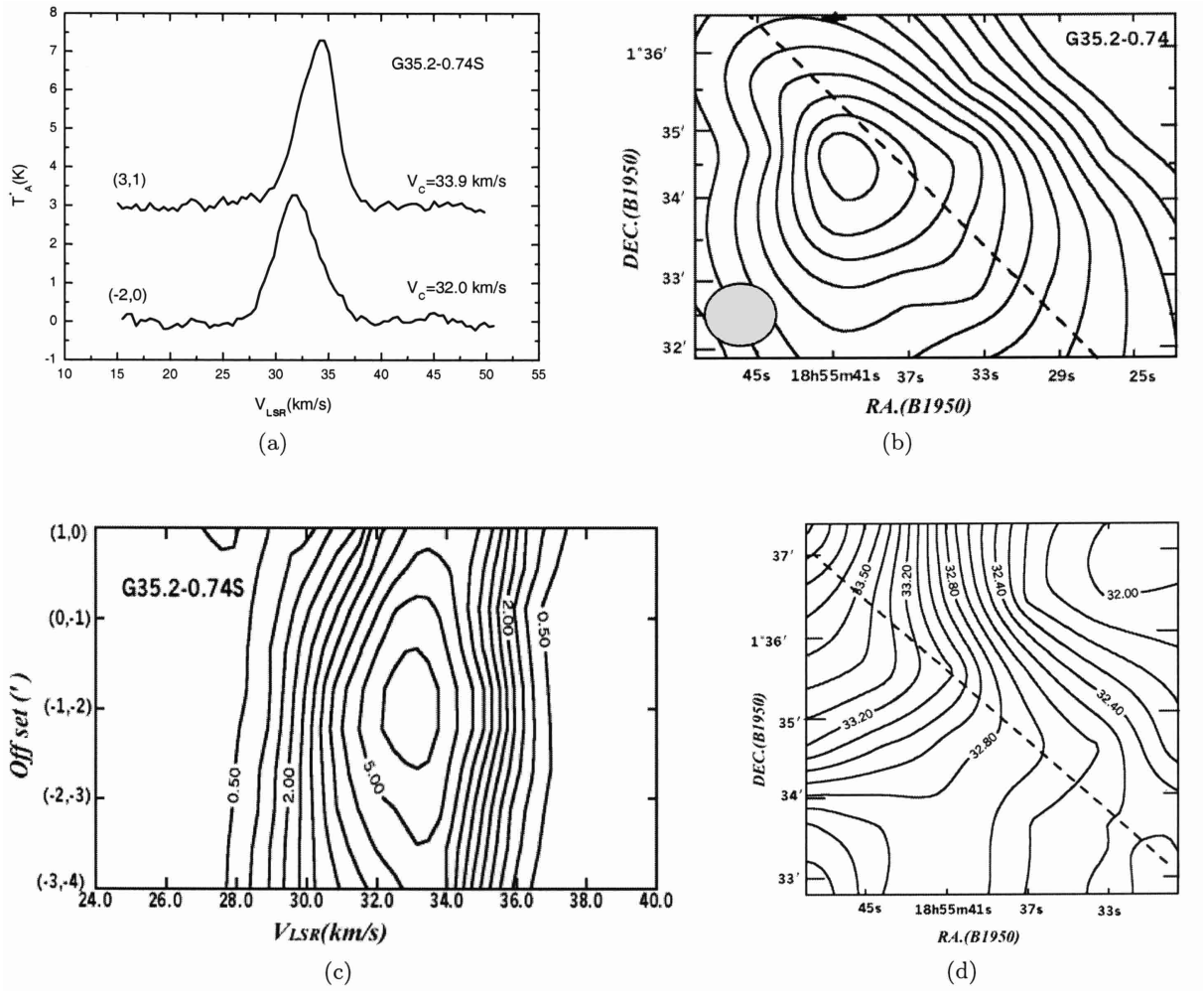

Fig. 4. G35.2–0.74S: panel **a)**: ^{13}CO $J = 1$–0 spectra; panel **b)**: contours of total ^{13}CO $J = 1$–0 emission. Contour lines begin from 55 K km s^{-1} with increasing steps of 5 K km s^{-1}. The cross denotes the IRAS position with its scale reflecting the uncertainty ellipse; panel **c)**: position versus velocity plot; panel **d)**: line center velocity contours.

Table 2. Parameters of mapped sources.

SOURCE	a ($'$)	b ($'$)	size (pc)	τ_{13}	T_{13} (K)	N_{13} (10^{15})	τ_{18}	T_{18} (K)	N_{18} (10^{15})	n_{H_2} (cm^{-3})	M_{core} ($M_\odot$)
06291+0421	3.5	3	0.8	.40	16.1	5.2	···	···	···	940	53
07207–1435	3	2	1.9	.30	12.4	3.4	···	···	···	260	220
G35.2–0.74S	7	5	1.7	···	···	···	.14	18.5	2.9	1400	840
K47	5	4	3.3	···	···	···	.07	12.9	1.2	290	1300
19282+1814	10	4	1.8	3.11	18.2	40.3	···	···	···	3250	2400
10877–0094	4.5	3.5	3.0	.17	43.2	8.3	···	···	···	400	1900
23133+6050	3.5	2	2.2	.07	61.2	4.5	···	···	···	290	390
23592+6716	4	3.5	0.7	.25	13.7	4.0	···	···	···	830	51

red but the spectral slopes are different, showing their different evolutionary status or varying environment.

G35.2–0.74S: the velocity gradient is 0.36 km s^{-1}/pc. A rotation with spin angular velocity 1.2×10^{-14} s^{-1} can account for the line center velocity shift. IRAS 18556+0136 is $2'$ away from the core on the north. In the southern part of the core there is a stellar image without a corresponding IRAS source (Dent et al. 1984).

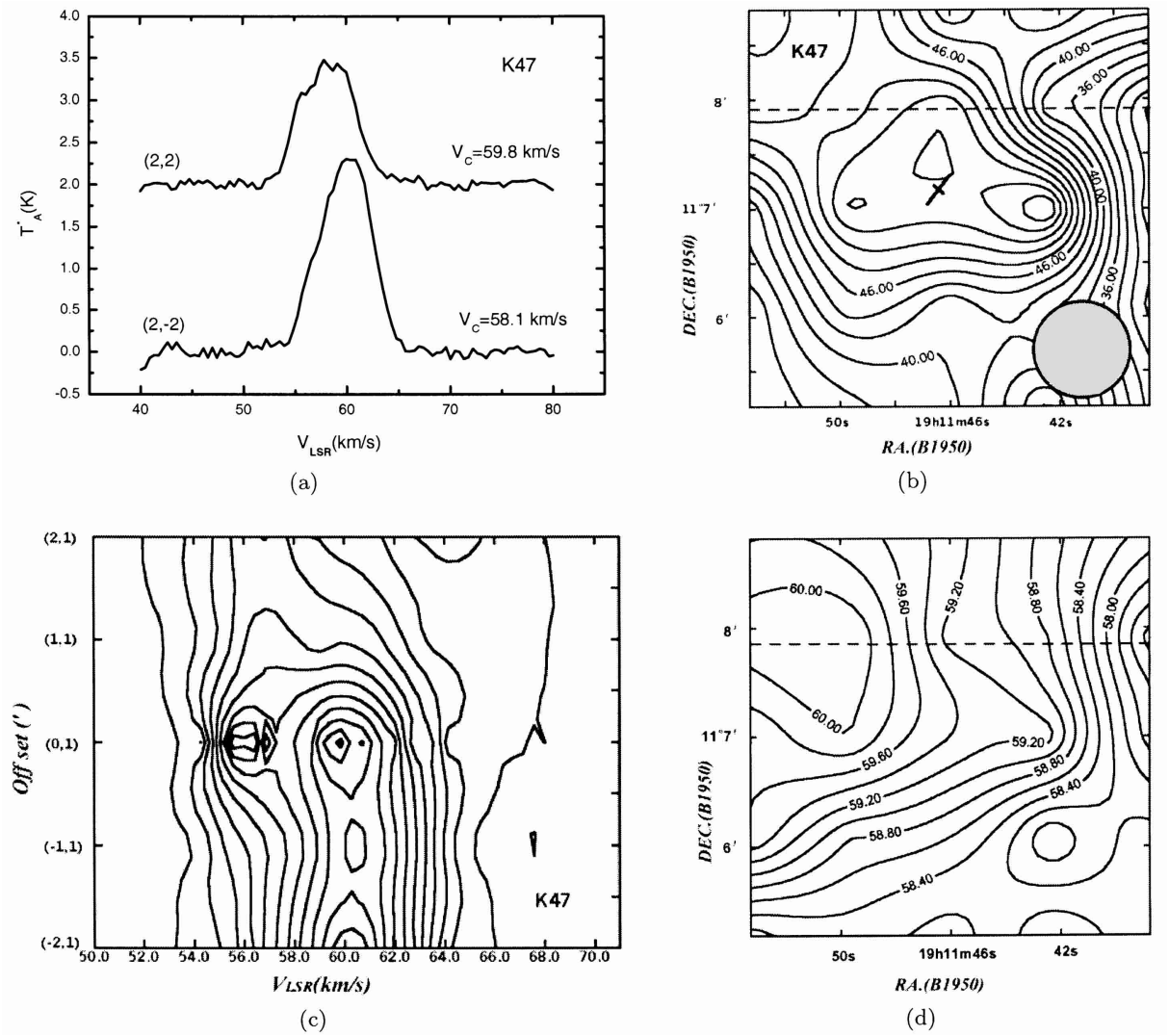

Fig. 5. K47: panel **a)**: ^{13}CO $J = 1$–0 spectra; panel **b)**: contours of total ^{13}CO $J = 1$–0 emission. Contour lines begin from 26 K km s^{-1} and end at 52 K km s^{-1}, with increasing steps of 2 K km s^{-1}. The cross denotes the IRAS position with its scale reflecting the uncertainty ellipse; panel **c)**: position versus velocity plot; panel **d)**: line center velocity contours.

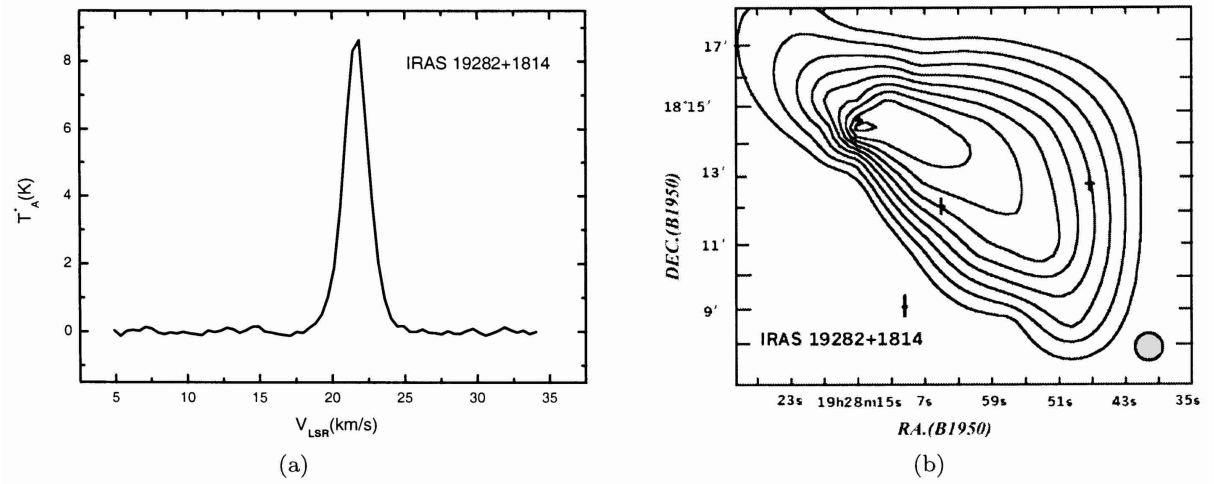

Fig. 6. IRAS 19282+1814: panel **a)**: ^{13}CO $J = 1$–0 spectra; panel **b)**: contours of total ^{13}CO $J = 1$–0 emission. Contour lines begin from 35 K km s^{-1} with increasing steps of 5 K km s^{-1}. Crosses denote IRAS sources with their scales reflecting the uncertainty ellipse.

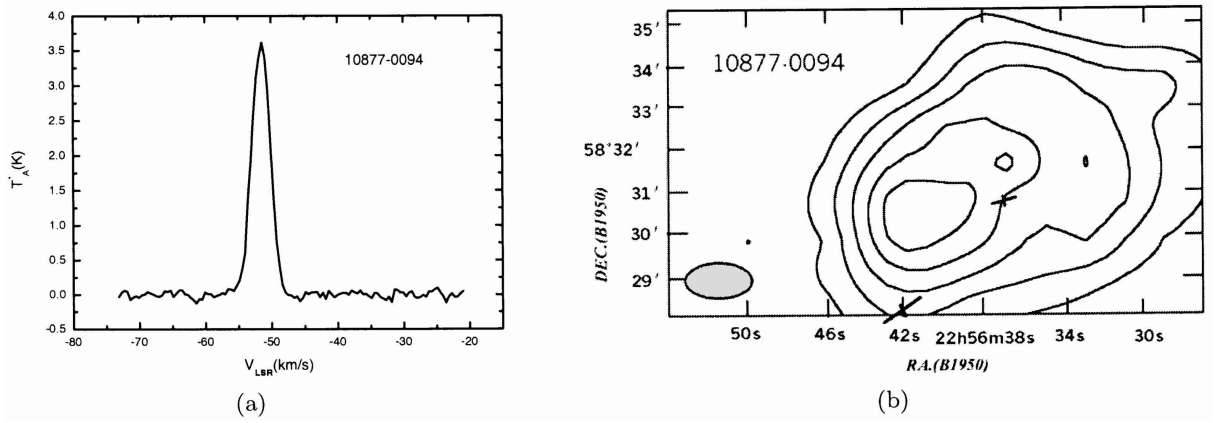

Fig. 7. 10877–0094: panel **a)**: ^{13}CO $J = 1$–0 spectra; panel **b)**: contours of total ^{13}CO $J = 1$–0 emission, contour lines begin from 40 K km s^{-1} with increasing step of 10 K km s^{-1}. Crosses denote IRAS sources with their scales reflecting the uncertainty ellipse.

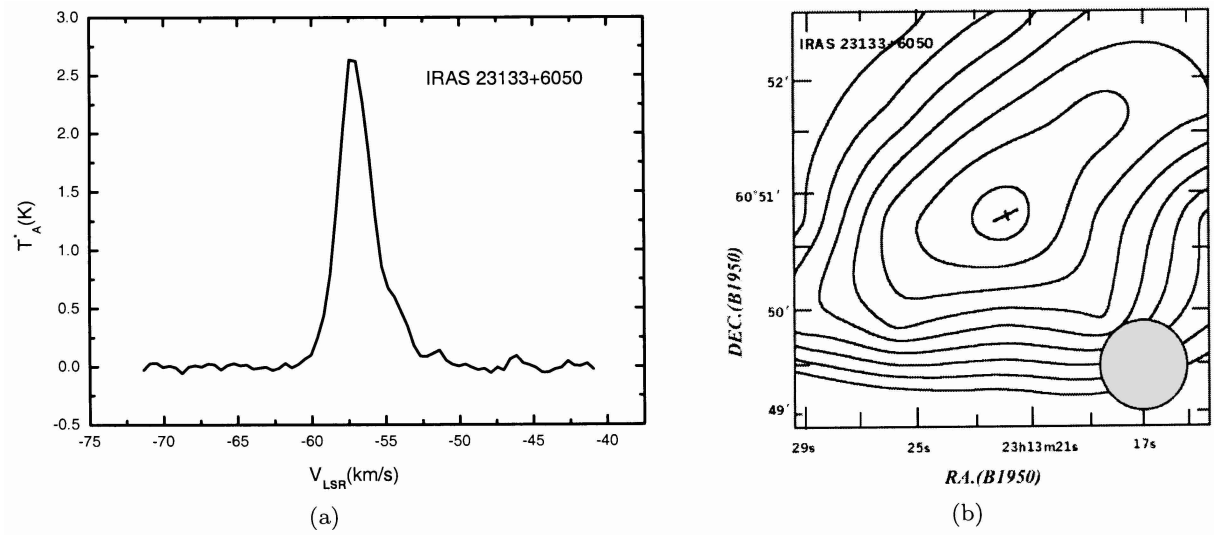

Fig. 8. IRAS 23133+6050: panel **a)**: ^{13}CO $J = 1$–0 spectra; panel **b)**: contours of total ^{13}CO $J = 1$–0 emission. Contour lines begin from 16 K km s^{-1} with increasing steps of 2 K km s^{-1}. The cross denotes the IRAS source with its scale reflecting the uncertainty ellipse.

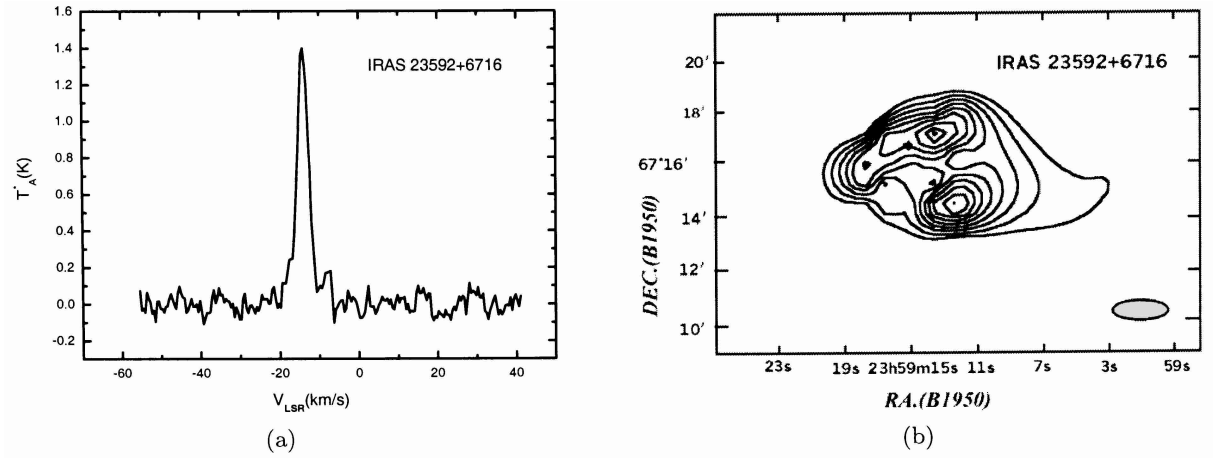

Fig. 9. IRAS 23592+6717: panel **a)**: ^{13}CO $J = 1$–0 spectra; panel **b)**: contours of total ^{13}CO $J = 1$–0 emission. Contour lines begin from 16 K km s^{-1} with increasing steps of 2 K km s^{-1}. The cross denotes the IRAS source with its scale reflecting the uncertainty ellipse.

K47: there are three clumps within the core region. The velocity gradient from east to west is 0.67 $\mathrm{km\,s^{-1}/pc}$ (Fig. 5d). A rotation with angular velocity 2.2×10^{-14} $\mathrm{s^{-1}}$ can account for it.

IRAS 19282+1814: four IRAS sources fall within the mapping region. IRAS 19282+1814 is the brightest and is located at the peak. There are 82 2MASS sources within $1'$ of the IRAS 19282+1814. These sources have different color indices and brightness.

10877–0094: the ^{13}CO $J = 1$–0 emission peak is at the south-east of IRAS 22566+5830 (Fig. 6b) and north of another IRAS source.

IRAS 23133+6050: the ^{13}CO $J = 1$–0 spectra (Fig. 8a) present red wings, which was also seen in the CO $J = 2$–1 lines. IRAS 23133+6050 is located at the emission peak in the core. Its contours agree well with the result of CO $J = 2$–1 observations (Wu et al. 2000).

IRAS 23592+6716: there are at least two clumps in the core region. IRAS 23592+6716 is near the northern peak.

Acknowledgements. We are grateful to F. Han, C. Lei, J. Sun, L. Wang and all the staff of Qinghai Station of PMO for their assistance in the observations. We also thank the referee and Maohai Huang for helpful comments or discussion. This publication makes use of data products from the 2MASS, which is a joint project of the University of Massachusetts and the Infrared Processing and Analysis Center/California Institute of Technology, funded by the NASA and NSF. This project is supported by G1999075405 of NKBRSF, 19773002 of the NSFC and the United Astronomy Lab. of CAS.

References

Beichman, C. A., Myers, P. C., Emerson, J. P., et al. 1986, ApJ, 307, 337
Brand, J., Cesaroni, R., Caselli, P., et al. 1994, A&AS, 103, 541
Bronfman, L., Nyman, L.-A., & May, J. 1996, A&AS, 115, 81
Casoli, F., Dupraz, C., Gerin, M., Combes, F., & Boulanger, F. 1986, A&A, 169, 281
Chan, S. J., Henning, T., & Schreger, K. 1996, A&AS, 115, 285
Churchwell, E. B. 1993, Observations of Newly Formed Massive Stars, in Massive stars: Their Lives in the Interstellar Medium, ed. J. P. Cassinell, & E. B. Churchwell (San Francisco: ASP) 35
Comoretto, G., Palagi, F., Cesaroni, R., et al. 1990, A&AS, 84, 179
Dent, W. R. F., Little, L. T., & White, G. J. 1984, MNRAS, 210, 173
Henning, Th., Pfau, W., & Altenhoff, W. J. 1990, A&A, 227, 542
Kutner, M. L., & Ulich, B. L. 1981, ApJ, 250, 341
Lada, C. J. 1985, ARA&A, 23, 267
Lada, E. A. 1992, ApJ, 393, L25
Li, W., Evans, N. J. II, & Lada, E. A. 1997, ApJ, 488, 277
Myers, D. C., Linke, R. A., & Benson, P. J. 1983, ApJ, 264, 517
Shepherd, D. S., & Churchwell, E. 1996, ApJ, 472, 225
Tatematsu, K., Umemoto, T., Kameya, O., et al. 1993, ApJ, 404, 643
Wood, D. O. S., & Churchweel, E. 1989, ApJ, 340, 265
Wynn-Williams, C. G. 1982, ARA&A, 20, 587
Wouterloot, J. G. A., & Brand, J. 1989, A&AS, 80, 149
Wu, Y., Huang, M., & He, J. 1996, A&AS, 115, 283
Wu, Y., Zhang, Q., Chen, H., Yang, C., & Ho, P. T. P. 2000b, preprint
Zhang, Q., Ho, P. T. P., & Ohashi, N. 1998, ApJ, 494, 636
Zhou, S. 1999, Low Mass Star Formation, in Millimeter-wave Astronomy: Molecular Chemistry & Physics in Space, ed. W. F. Wall, A. Carraminana, L. Carrasco, & P. F. Goldsmith (Kluver Academic Publishers), 199